PAPER

Check for updates

Poly(butylene 2,5-furandicarboxylate) copolyester obtained using 1,6-hexanediamine with high glass transition temperature

Ying Wang,[ab] Kunmei Su,†[*b] Chengzhi Liu[c] and Zhenhuan Li 🔟 †[*c]

A series of furan-based poly(ester amide)s, namely poly(butylene 2,5-furanoate)-*co*-(hexamethylene furanamide) (PBA$_s$F), were synthesized by partially substituting 1,4-butanediol (BDO) with linear hexamethylene diamine (HMDA). The introduction of amide bonding units enhances the intermolecular hydrogen bonding and intermolecular interaction forces, while the incorporation of flexible fragments results in a significant improvement in the thermal stability and mechanical properties of PBA$_s$F. PBA$_{20}$F exhibited an almost 50% increase in glass transition temperature, a mild improvement in tensile modulus of elasticity and tensile strength, and a tolerable decrease in elongation at break. Notably, the increased absorption in the UV wavelength range of PBA$_s$F is enhanced due to the increase in amide bonding, which increases UV degradability. Additionally, the discovery of treatment methods with excellent performance in dye rejection is another important aspect.

1 Introduction

Furan dicarboxylic acid-based polyesters are important substitute materials for terephthalic acid polyesters. However, poly(ethylene terephthalate) (PET) is currently one of the most highly produced and widely used polyester materials. It has excellent physical properties, good processability and the more important advantage of low cost in industrial production, making it ideal for various applications such as fibers, bottles and packaging material manufacturing.[1] However, PET is predominantly produced using non-renewable oil resources.[2,3] 2,5-Furandicarboxylic acid (FDCA) is a promising bio-based alternative to terephthalic acid (PTA) and has been identified by the U.S. Department of Energy as one of the 12 most promising bio-based platform compounds for bio-based aromatic chemicals.[4,5] FDCA and its derivatives are commonly utilized in the synthesis of bio-based polyurethanes, polyamides and, in particular, polyesters. Poly(butylene 2,5-furandicarboxylate) (PBF) has been found to be a bio-based and biodegradable polyester that exhibits excellent thermal stability and mechanical strength,[6] which make it a potential alternative to poly(butylene terephthalate) (PBT). Used as a packaging material, polyesters are usually required to have

a high glass transition temperature (T_g), which determines the material's processing and use properties, and it is an important characteristic parameter of polymeric materials. However, the low T_g of PBF seriously affects the performance of the product and greatly limits its application. In order to further expand its applications, cost-competitive renewable plastics are developed. Copolymerization with various diacids or diols has been investigated to improve the toughness and ductility of PBF,[7–11] but the tensile strength, modulus, and glass transition temperature are often significantly sacrificed.[12,13] The thermal stability of the material did not change significantly when copolymerized with PBF at low copolymer monomer content. Thus, developing a copolymer that enhances the thermal properties of PBF while retaining its original toughness and ductility is essential.

In recent years, studies have been conducted to develop some new poly(ester amides) with the excellent thermal, mechanical and biodegradable properties by incorporating amino-containing monomers into the polyester structure. The introduction of amide bonds leads to the formation of intermolecular hydrogen bonds (HBs), resulting in an increase in intermolecular interactions and a decrease in the mobility of the polymer chains, thus improving their thermal properties and mechanical strength,[14,15] the methylene unit, on the other hand, increases chain activity and increases elongation at break. The introduction of HBs under the combined action of both is an effective method to prepare high strength, high tenacity, and even high T_g polymer materials. Therefore poly(ester amide) containing ester and amide groups has received a lot of attention as a new and promising material.[15–22] FDCA-based poly(ester amides) have gained attention as a new and promising material due to their high strength, tenacity, and

[a]*State Key Laboratory of Separation Membranes and Membrane Processes/National Center for International Joint Research on Separation Membranes, Tiangong University, Tianjin, 300387, China*

[b]*School of Chemical Engineering and Technology, Tiangong University, 300387, Tianjin, China. E-mail: sukunmei@tiangong.edu.cn; Fax: +86 022 8395055; Tel: +86 022 8395055*

[c]*School of Materials Science and Engineering, Tiangong University, Tianjin, 300387, PR China. E-mail: lizhenhuan@tiangong.edu.cn*

† Authors equivalently contribute to this work.

potential for high glass transition temperature.[19,20,23] Amides can form the intermolecular hydrogen bonds, increasing intermolecular forces and improving thermal properties. Lips et al.[24] reported the improved mechanical properties of poly(-ester amides) after the introduction of amide bonds compared to the corresponding polymers or amide-free copolymers, demonstrating the potential of PBFA materials to combine the good properties of polyesters and polyamide.

Nanofiltration membranes have gained significant popularity in various applications such as dye removal, heavy metal ion separation, and desalination, which can be attributed to their cost-effectiveness, low energy consumption, as well as their high efficiency and selectivity.[33,34] In the realm of separation membrane preparation, polymeric materials are commonly utilized due to their favorable thermal and mechanical properties, however, there have been limited studies conducted on the utilization of furan-based polyester materials for membrane applications in aqueous media nanofiltration. The amide-modified furan-based copolyesters, known for their remarkable mechanical and thermal properties, offer potential advancements and expansions in the field of separation membranes. The treatment of dyeing wastewater is crucial due to the significant increase in its generation from the high demand for textiles. Effective treatment methods are necessary to mitigate the negative environmental and human health impacts associated with untreated or poorly treated dyeing wastewater.

Against this backdrop, we propose a simple yet innovative approach to design PBF copolyesters with the high glass transition temperatures and excellent mechanical properties, which is expected to significantly expand the practical applications of PBF copolyesters. A series of furan-based poly(ester-amide) polymers were synthesized by introducing 1,6-hexanediamine (HMDA) into PBF. Linear HMDA with amino and methylene groups was used to replace a portion of 1,4-butanediol (BDO) in the PBF main chain to synthesize poly(-butylene 2,5-furanoate)-co-(hexamethylene furanamide) (PBA$_s$F), where s denotes the amide content as a percentage of the copolyesters. The amino group serves as a functional group to form amide bonds, and the methylene group enhances chain flexibility. Due to the combined effects of intermolecular forces and microstructure of samples, it is expected that the glass transition temperature (T_g) of PBA$_s$F will increase. Meanwhile, the elastic tensile modulus will be increased without excessively sacrificing ductility, thus achieving both stiffness and good ductility. The produced polymer membranes underwent extensive testing to evaluate their wettability, permeability, and rejection of dye properties. Specifically, the effects of HMDA introduction on these properties were thoroughly characterized and discussed, focusing on the rejection and permeability characteristics of both PBF and PBA$_s$F polymer membranes.
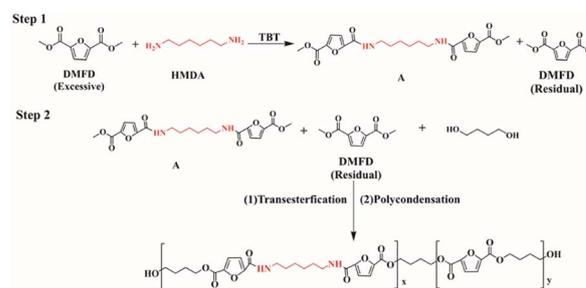
2 Experimental section

2.1. Materials

Dimethyl 2,5-furandicarboxylate (DMFD, 99.9%), Hubei Hongxin Ruiyu Fine Chemical Co. Tetrabutyl titanate (TBT), 1,6-hexamethylenediamine (HMDA), 1,4-butanediol (BDO) (99%), trifluoroacetic acid (CF$_3$COOH), Irganox 1010, 1,1,2,2-tetrachloroethane and deuterated trifluoroacetic acid (d-CF$_3$COOH) were purchased from Shanghai Maclean Biochemical Technology Co. Ltd. Phenol, Methyl Blue (MB) and Congo Red (CR), Tianjin Windship Chemical Reagent Co.

2.2. Synthesis of poly(ester amide)s

Scheme 1 illustrates the synthesis process, which involved two steps: amidation (step 1) and transesterification/polycondensation (step 2). The equipment commonly used for PBF synthesis was adequate for preparing PBA$_s$F samples within the necessary process parameter requirements. Table 1 provides a description of modified PBF with various amide-bond unit contents. The synthesis of PBA$_4$F (modified PBF with a 4 mol% amide-bond unit content) is described as follows: a mixture of DMFD (0.1 mol), HMDA (0.0036 mol), and TBT (0.8 wt% of DMFD) was prepared as a catalyst, and Irganox 1010 (0.8 wt% of DMFD) was added as an antioxidant. The mixture was continuously heated to 130 °C in dry nitrogen to initiate amidation until no methanol was distilled off. BDO (0.1764 mol) was then added to the reactor at a diester to diol molar ratio of 1 : 1.8. Methanol was collected as a by-product during this step. The transesterification reaction was performed at 180–190 °C for 4 h until the theoretical amount of methanol (~90%) was evaporated. The pressure was gradually decreased below 90 Pa, and the temperature was increased to 220 °C for 2 h, followed by a reduction in pressure to below 50 Pa for 3–5 h.

In the condensation polymerization process of furan-based polyesters and polyamides, the acylation and amination

Scheme 1 Synthetic process of PBA$_s$F.

Table 1 Composition of PBF, and PBA$_s$F based on them

Material	$n_{AF}{}^a$ (mol%)	$n_{AF}{}^b$ (mol%)	$[\eta]$
PBF	0	0	0.73
PBA$_4$F	4	3.92	0.75
PBA$_8$F	8	8.31	0.70
PBA$_{12}$F	12	11.32	0.68
PBA$_{16}$F	16	15.66	0.64
PBA$_{20}$F	20	19.00	0.64

[a] The percentage of HMDA in feed. [b] The percentage of AF contents in PBA$_s$F.

reactions are typically conducted at high temperatures ranging from 200 °C to 250 °C, which facilitate the reaction and product formation. However, the excessively high temperatures may cause decomposition or degradation of the products, making it necessary to adjust the temperature according to the specific reaction system and requirements. Furthermore, the reaction time, molar ratio of reactants, type and amount of catalyst, and other factors can also affect the reaction temperature and outcome. Hence, the synthesis process should be optimized and tailored to the specific conditions to achieve the desired reaction efficiency and product properties.

2.3. The preparation of polymer membranes

Firstly, PBF and its copolymer (amide ester) with a content of 18 wt% were dissolved in trifluoroacetic acid, resulting in a homogeneous solution upon thorough mixing. The resulting mixture was then applied onto a flat glass substrate using a scraping method. Next, the coated substrate was placed in a controlled environment of constant temperature and humidity to facilitate solvent evaporation. Finally, the prepared polymer membrane was peeled off from the glass surface to obtain the desired polymer membrane sample, and the membrane thickness of about 50 μm.

2.4. Characterization

Before characterization, all samples underwent a 5 hour drying process in a vacuum at 70 °C.

The chemical structure of PBA_sF copolymer was studied by recording ^1H NMR spectra on a Bruker spectrometer at 400 MHz using d-CF_3COOH as a solvent. To calculate the true fraction of the amide segment in the copolymers, the integrated intensities of the characteristic peaks were used. The Fourier transform infrared spectra were obtained in conjunction with a Nicolet iS50f Fourier transform infrared spectrometer with a scan range of 500–4000 cm^{-1} to characterize the structures of PBF and PBA_sF.

The intrinsic viscosity ($[\eta]$) of poly(ester amide)s was determined by using Ukrainian viscometer. A certain amount of dried Poly(ester amide)s was accurately weighed and dissolved in M1,1,2,2-tetrachloroethane : Mphenol = 1 : 1 into a mixed solution, the test temperature was 25 ± 0.1 °C, each concentration was measured three times, and then take the average.

The DSC 200F3 differential scanning calorimeter produced by NETZSCH GMBH was used to test the heat changes of the samples in different rising and cooling processes (nitrogen atmosphere: 50 ml min^{-1}). The testing process is as follows: under the protection of nitrogen, the cooling rate is reduced from 300 to 30 °C at 10 °C min^{-1}, and the samples are kept at 30 °C for 3 min, secondary heating rate 10 °C min^{-1} will increase the temperature from 30 to 300 °C, and recording the temperature rise and fall curves. The glass transition temperature (T_g) was taken as the median of the thermal transition step, and the melting temperature (T_m) was taken as the minimum of the endothermic peak.

The thermal stability of polymer was analyzed by thermogravimetric analysis (TGA). Test conditions: about 10 mg samples were placed in a crucible in a nitrogen atmosphere, with temperature rising from 30 to 800 °C at 10 °C min^{-1}. The stability of polymer was determined by the temperature T_d, max at the maximum weight loss rate.

The thermomechanical properties of the samples (10 mm × 6 mm × 0.2 mm) were tested in tensile mode using Dynamic Mechanical Analysis (DMA) (DMA242E, Germany). X-ray diffraction (XRD) spectra were recorded on an X-ray diffractometer (D8 DISCOVER, Germany) with a Cu Kα radiation source. A universal testing machine was used for tensile testing, the stretching rate of the sample (20 mm × 15 mm × 0.25 mm) was 5 mm min^{-1}, each sample was tested five times for average calculation. Ultraviolet-visible (UV-vis) absorption and reflection spectra were obtained by Ultraviolet-Visible-Near Infrared Spectrometer in the wavelength range of 240–800 nm. The thickness of the sample was ∼0.25 mm. A DSA-100 dynamic contact angle meter was used to characterize the hydrophilic properties of the co-polyester membrane surface. The samples were freeze-dried before the test, and each sample was measured at 5 different positions, and the average value was used as the measurement result.

2.5. Nanofiltration performance assessment

The porosity of the membranes was determined by weight method. The membrane porosity was expressed as in eqn (1):

$$\varepsilon(\%) = \left(\frac{W_w - W_d}{\rho A \delta} \right) \times 100 \tag{1}$$

where, W_w and W_d are the sample weights (g) in the wet and dry states, respectively. ρ is the density of distilled water (g cm^{-3}), A is the surface area of sample (cm^2) and δ is the thickness of wet membrane (cm).

The test was carried out in a staggered flow type water flux test device with a test pressure of 6 bar, and the received water was weighed every 10 min, and the data was measured in 6 groups and the average value was taken after the data was stabilized. Water flux calculation formula as in eqn (2):

$$J = \frac{V}{A \times \Delta t} \tag{2}$$

where J is the water flux (L $m^{-2} h^{-1}$), V (L) is the water volume, A (m^2) is the membrane area, and Δt (h) is the test interval time.

Methyl Blue (MB) and Congo Red (CR) were selected as the contaminants in the simulated separation test with a concentration of 50 ppm to test the membrane rejection performance of dyes. The test setup and parameters are the same as the pure water flux test procedure, with the dye rejection rate as in eqn (3):

$$R(\%) = \left(1 - \frac{C_1}{C_2} \right) \times 100 \tag{3}$$

where R represents the rejection rate (%), C_1 represents the dye concentration of the filtrate, and C_2 represents the dye concentration of pre-filtrate.

Refer to GB15979, GB8629, FZ/T01021-92 Japanese JIS, Japanese Nobalon, American AATCC100 antimicrobial

standards for testing. *Staphylococcus aureus* was used as a representative. Bacterial suspensions without membrane samples were used as controls. The number of microbial colonies on the medium was counted using the viable bacteria counting method. Bacterial inhibition rate (*T*%) was calculated according to eqn (4):

$$T(\%) = \frac{A - B}{A} \times 100 \qquad (4)$$

where *T* is the antimicrobial rate (%), *B* is the number of microbial colonies of PBF and PBA$_s$F, *A* is the number of microbial colonies of the blank control group.

3   Results and discussion

3.1.   Synthesis of amide-bond-modified PBF

PBA$_s$F samples containing amide-bonded units were synthesized by incorporating HMDA as a copolymer monomer, following the synthetic route depicted in Scheme 1. The introduction of amide bonds led to partial alteration of the polarity and microstructure of PBA$_s$F. An increase in the number of amide bonds caused the samples to exhibit a yellow colour. To expand the scope of material applications and enhance its aesthetics, the content of amide bonds was restricted to a maximum of 20 mol%. Using different monomers, PBA$_s$F with varying amide bond contents (0, 4, 8, 12, 16, and 20 mol%) were prepared (Table 1).

The characteristic viscosity [η] of a polymer is related to its molecular weight, where a higher molecular weight corresponds to a higher [η]. In the case of PBA$_s$F, the introduction of amide-bonded units can influence the molecular weight and therefore the [η] of the resulting polymer. At a low amide content of 4%, the slight increase in [η] may be due to the intermolecular hydrogen bonding between the amide and ester groups, which can lead to an increase in molecular weight. However, at higher amide contents, the decrease in [η] may be due to the fact that HMDA and BDO monomers have different reactivity, leading to a less efficient polymerization and a lower molecular weight. Therefore, the [η] of PBA$_s$F can be influenced by various factors such as monomer reactivity, reaction conditions, and the presence of specific functional groups.[25] The success of polymerization can be confirmed by ^{1}H NMR and FTIR spectra of PBA$_s$F samples. In the Fig. 1(b), the peak at 1716 cm^{-1} corresponds to the stretching vibration of the C=O bond in the ester segment, while the peak at 1137 cm^{-1} is due to the stretching vibration of the C–O bond in the ester group. The appearance of a new peak at 1653 cm^{-1} indicates the stretching vibration of the C–N bond in the amide segment, while the peaks at 1516 cm^{-1} and 3469 cm^{-1} correspond to the N–H bending and stretching vibrations, respectively, of the introduced amide group. These peaks are characteristic of amide bonds, and their presence confirms the successful incorporation of the amide segment into the polymer backbone.

The ^{1}H NMR spectrum of PBA$_s$F provides the information about the chemical environment of the protons in polymer. The Fig. 1(a) shows the possible assignment of the ^{1}H NMR peaks and their corresponding molecular structure. All signal peaks corresponding to the PBF unit were clearly visible,
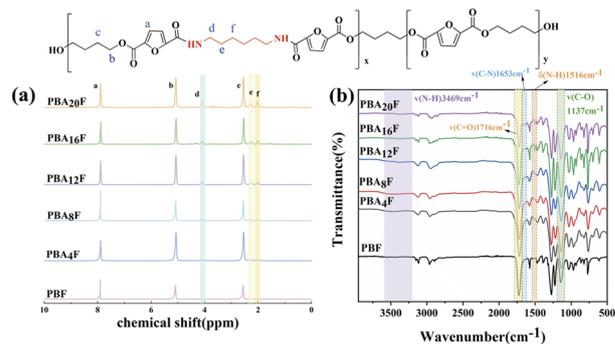

Fig. 1 (a) ^{1}H NMR spectra of PBF and PBA$_s$F, (b) FTIR spectra of PBF and PBA$_s$F.

together with the peak at 7.89 ppm (a) associated with a proton on the furan ring, and two more intense peaks from the PBF unit at 5.07 ppm (b) arising from a methylene adjacent to the oxygen atom, and at 2.54 ppm (c) from a proton next to the oxygen atom. For the (hexamethylene furanamide) (AF) segment, new signals associated with the esteramide sequence appear. The peak at 4.09 ppm (d) is attributed to the hydrogen on the methylene group attached to the amide proton, and the peaks at 2.26 ppm and 2.01 ppm correspond to protons at (e) and (f), respectively, slightly farther from the amino group. These ^{1}H NMR peaks provide evidence for the successful synthesis of PBA$_s$F and the incorporation of the amide segment into the polymer structure. The comparison with literature[26] data further confirms the success of polymerization.

To estimate the actual molar fraction of AF units, the copolymer composition (n_{AF}) was calculated according to eqn (5):

$$n_{AF}(\%) = \frac{I_d}{I_d + I_b} \times 100 \qquad (5)$$

The ratio of the peak areas in the ^{1}H NMR spectra of the amide-only (position d) and ester-only peaks (position b) is used to calculate the proportion of the amide content, and the calculated proportion is the proportion of the true composition of the polymer.

Based on the results obtained from ^{1}H NMR, it can be inferred that FDCA-based copolymers (ester amides) have been successfully synthesized. Wilsens *et al.*[27] pointed out that the intermolecular hydrogen bonds can be formed between the oxygen heteroatom on the furan ring and the hydrogen on the amide bond. However, this leads to a loss of resonance corresponding to the amide proton and the calculated value of the molar fraction of the A$_s$F segment obtained by integration being slightly lower than the theoretical value.

3.2.   Thermal properties

The thermal performance of PBA$_s$F was investigated through the use of DSC, TGA, and DMA testers, with results illustrated in Fig. 2 and 3. Additionally, detailed data is presented in Table 2.
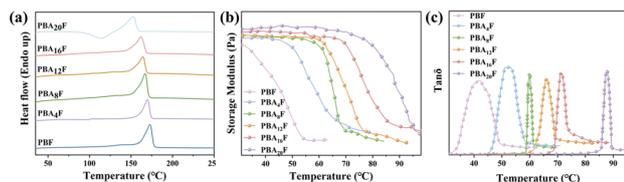
Fig. 2 (a) DSC second heating curves of PBF and PBA$_s$F, (b) storage modulus curves and (c) loss factor curves in DMA tests.
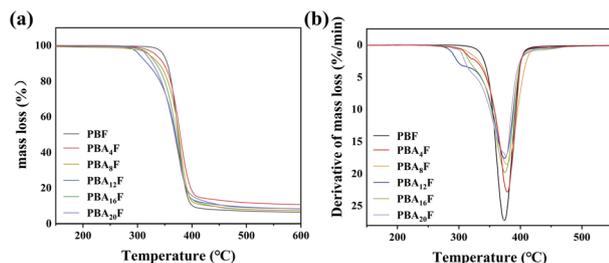

Fig. 3 (a) TGA and (b) derivative TGA curves of PBF and PBA$_s$F.

DSC has certain limitations in determining glass transition temperatures, which prompted the use of DMA to obtain storage modulus (E') and loss angle ($\tan \delta$) data versus temperature for copolyesters. The obtained DMA results are consistent with the DSC results presented in the Fig. 2 and Table 2, showing a single T_g in all copolyesters, indicating that the ester and ester-amide segments are miscible in the amorphous state. The T_g of PBA$_s$F increases notably with the increase in the number of amide groups, which is attributed to the ability of amide groups to form hydrogen bonds, leading to increased intermolecular interactions that limit the segmental motion of the copolyesters and reduce the mobility of the polymer chains.[14,18] Additionally, the strong hardening effect of the hydrogen bonding of the amide group also contributes to the observed increase in T_g. T_g represents the temperature at which the chain segments undergo coordinated molecular motion, therefore increases with the introduction of diamine content.

The regularity and rigidity of molecular chains are critical intrinsic factors that determine T_m of copolyesters.[28] As shown in Fig. 2(a), T_m decreases with increasing diamine content, which can be attributed to changes in chemical structure and hydrogen bonding, which influence chain rigidity and regularity. Several factors may account for this. Although

intermolecular hydrogen bonding typically increases the melting point, the introduction of long flexible AF segments lowers the melting point of copolyesters. Moreover, the decrease in T_m with increasing chain length of aliphatic diamines is caused by the increase in chain flexibility with an increase in methylene units, leading to a reduction in HBs and p–p stacking density.[29] Another factor contributing to the overall decrease in melting point is the different reactivity of BDO and HMDA, which leads to a decrease in molecular weight. At the same time, the introduction of amide groups disturbs the ordered arrangement of polymer molecules and reduces the degree of crystallization, which is one of the reasons for the decrease in the T_m of polymers.

The melt crystallization temperature (T_c) and enthalpy (ΔH_c) were collected from the cooling step. The glass transition temperature (T_g), melting temperature (T_m) and enthalpy (ΔH_m) were obtained during the second heating step.

The thermal degradation behaviour of PBF and PBA$_s$F samples is shown in Fig. 3. The temperatures at 5% weight loss (T_d) and at maximum weight loss (T_{dm}) are summarized in the Table 2. From the Table 2, it can be seen that T_{dm} increases slightly with increasing amine content while T_d tends to decrease. It is inferred that the bonding energy between different monomers during the copolymerization process varies greatly, unstable chemical bonds that are susceptible to pyrolysis are created. And the copolymerized monomers are not uniformly distributed in the polymer, which leads to local overheating or insufficient decomposition of the polymer during heating, while the amide bonding group plays a positive role in the thermal stability. Nevertheless, based on the reduced low T_m, the processable interval increases.

3.3. Crystallization properties

Due to the structural regularity and chain flexibility of the BDO groups, PBF exhibits semi-crystalline behaviour with good crystallinity.[30] However, when both components in copolyesters can crystallize, the crystallinity decreases with increasing content of the second component due to lattice incompatibility,[31] as observed in the Fig. 4(a). Interestingly, the cold crystallization area of PBA$_4$F is slightly elevated, indicating that the introduction of a small amount of amide bonding units may promote the cooling process during crystallization.[18] As the proportion of copolymer monomers becomes more homogeneous, the randomness of polymer chains hinders their ability to organize in the crystal structure, leading to a decrease in

Table 2 Thermal property of PBF and PBA$_s$F

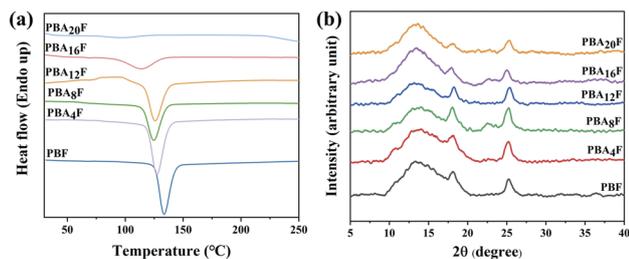| Sample	DSC					TG		DMA
	T_g (°C)	T_c (°C)	ΔH_c (J g^{-1})	T_m (°C)	ΔH_m (J g^{-1})	T_d (°C)	T_{dm} (°C)	T_α (°C)
PBF	40.3	133.2	50.51	170.1	49.3	347.8	373	41.9
PBA$_4$F	—	127.4	55.5	169.9	52.01	346.5	379.0	52.3
PBA$_8$F	60.4	125.8	41.72	167.1	37.18	345.2	377.6	59.8
PBA$_{12}$F	67.7	113.9	25.28	164.4	35.7	343.8	374.0	66.1
PBA$_{16}$F	76.4	101.5	26.95	152.9	28.51	343.4	374.6	71.3
PBA$_{20}$F	—	97.3	4.887	150.6	25.43	342.8	376.5	87.6

Fig. 4 (a) DSC first cooling scan curves of PBF and PBA$_s$F, (b) XRD patterns for PBF and PBA$_s$F.

crystallization ability to semi-crystalline or amorphous materials. The cold crystallization peak almost disappears at PBA$_{20}$F, suggesting that the introduction of a high number of amide bonding units suppresses the formation of nuclei during cooling and results in decreased crystallization ability, and thus the crystallization ability decreases to semi-crystalline or amorphous materials.

To complement the DSC results, X-ray diffraction (XRD) patterns of PBA$_s$F were obtained and presented in Fig. 4(b). Both PBF and PBA$_s$F exhibited the varying degrees of crystallinity, with the main diffraction peaks of PBF located at 2θ values of 12.6°, 18.1°, and 25.0°,[6] corresponding to the (001), (010), and (100) crystal planes, respectively. In the XRD patterns of PBA$_s$F, no new diffraction peaks were observed, indicating that no AF crystals were formed. The (010) and (100) peaks gradually weakened with increasing amide content at amide contents greater than 6%, indicating a decrease in the orientation of copolyesters in these planes and a gradual distribution of the crystalline planes uniformly within the membrane. These results are consistent with the trend observed in the DSC cooling curve, which suggest that the intensity of the diffraction peaks varied with the AF content.

3.4. Mechanical properties

Further investigation was conducted to analyse the effects of intermolecular hydrogen bonds (HBs) and flexible fragments on the mechanical properties of materials. Fig. 5 shows the tensile strain–stress curves obtained from the tests. The mechanical properties of copolyesters are determined by its intermolecular structure, forces and molecular weight.[32] The Fig. 5(c) reveals that the increase in amide bond content leads to the gradual improvement of mechanical properties due to the formation of a physical crosslinking network induced by HBs. The elastic modulus strength (E) and tensile strength (σ_y) of PBA$_s$F reach
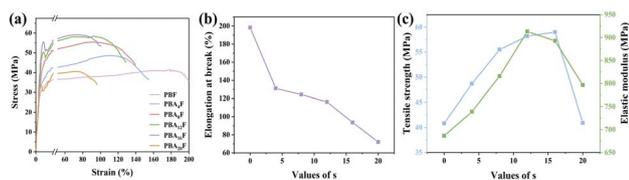
their peak at s of 12 (913.2 MPa) and 16 (59.1 MPa), respectively. This significant increase in tensile strength broadens the potential packaging applications of PBA$_s$F. However, as the amide content continues to increase, a decrease in intrinsic viscosity ($[\eta]$) and an increase in methylene unit content occur. The increased HBs cannot offset the negative effects of lower molecular weight and methylene flexible fragments on mechanical properties, leading to lower E and σ_y. At the same time, elongation at break (ε_b) decreases with the increase of amide bond content. The enhancement of intermolecular HBs with increasing amide bond content restricts the motion of polymer chains, resulting in decreased elongation at break (Table 3).

3.5. Optical properties of PBA$_s$F

Packaging light avoidance reduces direct damage to food primarily by absorbing or reflecting light. Therefore, it is essential to detect the absorbance and reflectance of polyesters in the UV and visible wavelength range to maximize the protective benefits. Fig. 6(a) and (b) depict the reflectance and absorbance of PBF and PBA$_s$F, respectively, in the UV-vis test. PBF exhibits the excellent reflectance in the visible wavelength range of 400–760 nm and strong absorbance in the UV wavelength range of 280–400 nm. PBA$_s$F, on the other hand, demonstrates an increased absorbance with an increase of amide bonding, rendering it more susceptible to degradation under UV. Conversely, its reflectivity declines with the rise of amide bonding.

3.6. Antimicrobial and nanofiltration membrane properties of PBA$_s$F polymer membranes

Considering the crucial factors of melting point, loss of elongation at break, and decrease in molecular weight, PBA$_s$F polymer membrane with different HMDA composition ratios (s = 0, 4, 8, 12) were chosen for the production of polymer membrane using solvent evaporation. These selected PBA$_s$F compositions were specifically targeted to rejection and antimicrobial testing in order to establish a solid groundwork for future applications.

It can be observed in Fig. 7. The produced nanofiltration membrane is an asymmetric membrane, the upper surface of the membrane is denser compared to the lower surface of the nanofiltration membrane, and the surface of the lower membrane is a more uniform spherical porous structure. The intermediate support layer is similar to the lower surface, both of which are spherical porous structure, which helps to increase

Fig. 5 (a) Tensile curves of PBF and PBA$_s$F, (b) elongation at break of PBF and PBA$_s$F, (c) tensile strength and elastic modulus of PBF and PBA$_s$F.

Table 3 Mechanical properties

Material	E [MPa]	σ_y [MPa]	ε_b [%]
PBF	686.55 ± 23.2	40.835 ± 2.1	198.35 ± 9.8
PBA$_4$F	738.85 ± 13.8	48.75 ± 1.8	131.15 ± 3.5
PBA$_8$F	815.95 ± 25.6	55.55 ± 2.0	124.25 ± 5.2
PBA$_{12}$F	913.25 ± 22.1	58.25 ± 2.3	116.35 ± 7.5
PBA$_{16}$F	892.95 ± 27.6	59.015 ± 1.4	93.65 ± 3.6
PBA$_{20}$F	796.55 ± 23.7	40.925 ± 1.8	72.5 ± 4.4

Fig. 6 UV testing curves: (a) reflectance, (b) absorbance.

Fig. 8 (a) The retention rates and (c) the photos of MB and CR at 10 ppm, (b) the retention rates and (d) the photos of MB and CR at 50 ppm.

the filtration area. And from the Fig. 7, it can be seen that the connection between spherical is more dense, not easy to increase the flux.

The rejection rates of both PBF and PBA$_s$F membranes for the dyes MB and CR can be observed to exceed 90% at a concentration of 10 ppm, as depicted in Fig. 8. Particularly, PBA$_4$F achieved a remarkable rejection rate of 95.6%. Even at a higher concentration of 50 ppm, the rejection rate remains above 65%. Digital photographs in Fig. 8(c) and (d) present the rejection of MB and CR at different concentrations, wherein 1, 2, 3, 4, and 5 represent the pre-filtration stock solution and the liquids rejected by the PBF, PBA$_4$F, PBA$_8$F, and PBA$_{12}$F membranes, respectively. The rejection performance of the nanofiltration membranes for the dyestuffs is mainly influenced by the Donnan-effect and the pore size sieving effect. The relative molecular mass (M_r) of MB is 799.80, while that of CR is 696.68, resulting in a slightly lower rejection rate for CR compared to MB, but it still remains at a high level. These results provide evidence that both PBF and PBA$_s$F membranes can effectively retain dyes.

The Fig. 9 depicts the water flux observed in the prepared polymeric separation membrane when subjected to a pressure of 6 bar. Water flux is typically influenced by the porosity of the membrane and the wettability characteristics of the material. From the Fig. 9(a) graph, it is evident that the hydrophilicity of the polymer membrane exhibits an upward trend as HMDA content increases. However, at $s = 4$, the water flux is slightly impeded by the porosity, leading to a minor decrease in water flux. Nonetheless, as the porosity and hydrophilicity are further
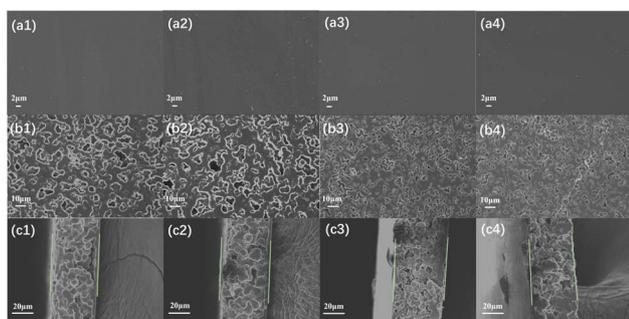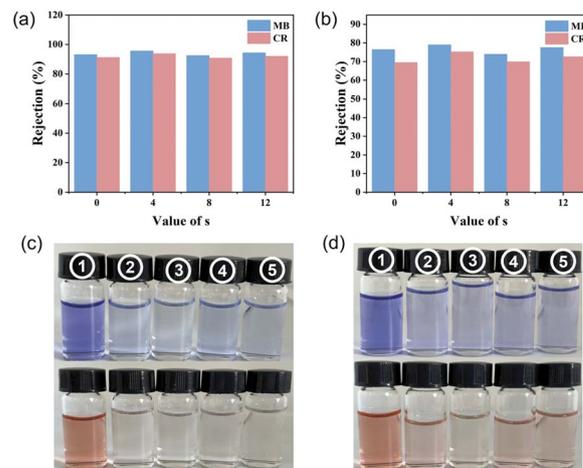
increased at $s = 8$ and $s = 12$, a marginal improvement in water flux is observed. However, it should be noted that the overall water flux remains relatively inadequate despite these variations.

Some commonly used polymer membranes such as polyacrylonitrile (PAN),[35] poly(phenylene sulfone) (PPSU),[36] polyvinyl chloride (PVC),[37] polyethylene glycol (PES)[38] bare membrane on the *Staphylococcus aureus* antimicrobial poor, easy to be broken down by microorganisms erosion and thus reduce the service life, if want to increase its antimicrobial properties, and through the introduction of antimicrobial materials will increase the cost. Although PET has 53.8% antimicrobial activity against *Staphylococcus aureus*,[39] the non-degradable nature of the PET material and the unsustainable nature of the raw materials used in its production are detrimental to the environment. Therefore, it is important to find polymer films that have good antimicrobial properties and are sustainable.

The observed growth and antibacterial properties of *S. aureus* colonies on solid medium are illustrated in Fig. 10, wherein 1, 2, 3, 4, and 5 represent the blank control group and PBF, PBA$_4$F, PBA$_8$F, PBA$_{12}$F membranes, respectively. Our findings indicate that PBF possesses inherent antibacterial properties. However, the magnitude of this property is relatively
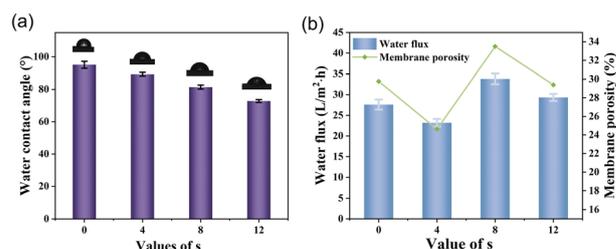

Fig. 7 (a) The upper surface, (b) the lower surface, and (c) the cross-section of the PBF and PBA$_s$F membranes. 1, 2, 3, 4 represent the PBF, PBA$_4$F, PBA$_8$F, and PBA$_{12}$F membranes, respectively.

Fig. 9 (a) Water contact angle of PBF and PBA$_s$F membrane, (b) porosity and water flux of PBF and PBA$_s$F membranes.
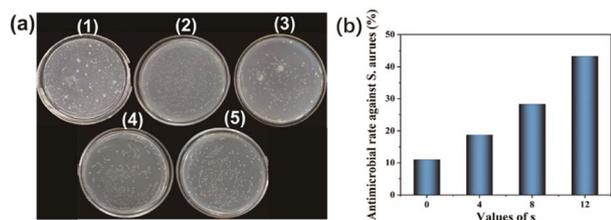
Fig. 10 Photos of *S. aureus* colony (a). (b) Antimicrobial rate of PBF and PBA$_s$F against *S. aureus*.

low, with a calculated antibacterial rate of only 11.0% as determined by eqn (4). In contrast, the inclusion of amide in PBA$_s$F ($s = 4, 8, 12$) enhances its antibacterial property, with an increasing trend observed as the amide concentration rises. Specifically, the supplemented amide content positively correlates with the observed efficacy against *S. aureus*, as depicted in Fig. 10(b).

4 Conclusions

In this study, we synthesized a series of furan-based poly(ester amide) copolymers PBA$_s$F, by introducing 1,6-hexanediamine into PBF, which exhibit outstanding mechanical, thermal properties. The structures and the presence of hydrogen bonds were confirmed by ^{1}H NMR spectroscopy and FTIR spectroscopy. The resulting PBA$_{20}$F displayed a much higher glass transition temperature (87.6 °C) than PBF, nearly 50% higher, due to the intermolecular hydrogen bonding interactions. Additionally, we found that the small amount (4 mol%) of amide-bonded units could slightly promote crystallization, whereas the maximum thermal degradation temperature (T_{dm}) increased slightly, but T_m tended to decrease due to the decrease in [η] and molecular chain regularity, resulting in a wider processable range for the polyester. Owing to the combined effects of intermolecular hydrogen bonding forces and flexible fragments, the copolyester showed the excellent values of tensile strength and elastic modulus, while the elongation at break was slightly reduced, its overall performance remained relatively good. Furthermore, the absorption of PBA$_s$F enhances with an increase in amide bonding, thus increasing its degradability under UV light, making it suitable for use in biodegradable packaging. This study provides a promising approach for designing polyester amides with great mechanical properties, as well as high glass transition temperatures. For the modified furan polyesters herein can be used to make higher quality products, such as high strength fiber materials, to improve the service life and safety of the products. At the same time, it can replace the non-degradable plastics and chemical fibers, and has a certain role in promoting environmental protection.

PBA$_s$F with $s = 0, 4, 8, 12$ was selected to produce the membrane by solvent evaporation method, and it was found that the inhibitory effect of polymer membrane on bacteria, showed an increasing trend with the increase of HMDA content. The water flux was slightly increased compared to PBF, and the

rejection performance of PBF and PBA$_s$F membrane was also maintained at higher concentrations for anionic dyes of different molecular weights. Overall, the proposed membrane in the paper has the property of inhibiting the growth of bacteria itself, which means that it is able to effectively reduce the adhesion and multiplication of bacteria on the membrane surface and reduce the contaminability, which is a property that is not available in the currently understood membranes. Secondly, the hydrophilicity of the proposed membrane is slightly increased compared to other membranes. This means that it is able to better adsorb and transfer water molecules, which contributes to the improvement of water permeability and flux, and subsequently only needs to adjust its pore size to improve water flux. Finally, the proposed membrane was able to maintain a high retention performance at high concentrations.

Author contributions

All authors have given approval to the final version of the manuscript.

Conflicts of interest

The authors declare no competing financial interest.

Acknowledgements

Notes and references

1 R. Wei and W. Zimmermann, *Microb. Biotechnol.*, 2017, **10**, 1302–1307.
2 P. K. Sampath Gunukulaa and R. Anex, *Chem. Eng. Res. Des.*, 2016, **107**, 24–33.
3 A. Gandini, T. M. Lacerda, A. J. F. Carvalho and E. Trovatti, *Chem. Rev.*, 2015, **116**, 1637–1669.
4 G. Z. Papageorgiou, D. G. Papageorgiou, Z. Terzopoulou and D. N. Bikiaris, *Eur. Polym. J.*, 2016, **83**, 202–229.
5 M. Konstantopoulou, Z. Terzopoulou, M. Nerantzaki, J. Tsagkalias, D. S. Achilias, D. N. Bikiaris, S. Exarhopoulos, D. G. Papageorgiou and G. Z. Papageorgiou, *Eur. Polym. J.*, 2017, **89**, 349–366.
6 J. Zhu, J. Cai, W. Xie, P.-H. Chen, M. Gazzano, M. Scandola and R. A. Gross, *Macromolecules*, 2013, **46**, 796–804.
7 G. Wang, M. Jiang, Q. Zhang, R. Wang, X. Tong, S. Xue and G. Zhou, *Polym. Degrad. Stab.*, 2017, **143**, 1–8.
8 B. Wu, Y. Xu, Z. Bu, L. Wu, B.-G. Li and P. Dubois, *Polymer*, 2014, **55**, 3648–3655.
9 J. C. Morales-Huerta, C. B. Ciulik, A. M. de Ilarduya and S. Muñoz-Guerra, *Polym. Chem.*, 2017, **8**, 748–760.

10 S. Peng, B. Wu, L. Wu, B.-G. Li and P. Dubois, *J. Appl. Polym. Sci.*, 2017, **134**, 44674–44684.

11 H. Hu, R. Zhang, J. Wang, W. B. Ying and J. Zhu, *ACS Sustainable Chem. Eng.*, 2018, **6**, 7488–7498.

12 J. Wang, X. Liu, J. Zhu and Y. Jiang, *Polymers*, 2017, **9**, 305.

13 A. Shen, G. Wang, J. Wang, X. Zhang, X. Fei, L. Fan, J. Zhu and X. Liu, *Eur. Polym. J.*, 2021, **147**, 110317.

14 Y. Hao, M. Chen, J. Zhao, Z. Zhang and W. Yang, *Ind. Eng. Chem. Res.*, 2013, **52**, 6410–6421.

15 M. Kluge, L. Papadopoulos, A. Magaziotis, D. Tzetzis, A. Zamboulis, D. N. Bikiaris and T. Robert, *ACS Sustainable Chem. Eng.*, 2020, **8**(29), 10812–10821.

16 A. Soleimani, S. Drappel, R. Carlini, A. Goredema and E. R. Gillies, *Ind. Eng. Chem. Res.*, 2014, **53**, 1452–1460.

17 H. Gao, H. Liu, J. He and Y. Bai, *J. Mater. Sci.*, 2020, **56**, 4922–4939.

18 H. Gao, Y. Bai, H. Liu and J. He, *Ind. Eng. Chem. Res.*, 2019, **58**, 21872–21880.

19 M. Kluge, H. Rennhofer, H. C. Lichtenegger, F. W. Liebner and T. Robert, *Eur. Polym. J.*, 2020, **129**, 109622.

20 M. Kluge, D. N. Bikiaris and T. Robert, *Eur. Polym. J.*, 2019, **120**, 109195.

21 L. Papadopoulos, P. A. Klonos, M. Kluge, A. Zamboulis, Z. Terzopoulou, D. Kourtidou, A. Magaziotis, K. Chrissafis, A. Kyritsis, D. N. Bikiaris and T. Robert, *Polym. Chem.*, 2021, **12**, 5518–5534.

22 L. Sangroniz, M. A. Hillmyer and Y. J. Jang, *Polym. Chem.*, 2022, **13**, 3882–3891.

23 D. Maniar, F. Silvianti, V. M. Ospina, A. J. J. Woortman, J. van Dijken and K. Loos, *Polymer*, 2020, **205**, 122662.

24 P. A. M. Lips, R. Broos, M. J. M. van Heeringen, P. J. Dijkstra and J. Feijen, *Polymer*, 2005, **46**, 7823–7833.

25 W. Q. Du, T. Fu, X. L. Li, Y. Li, C. Deng, X.-L. Wang and Y.-Z. Wang, *ACS Sustain. Chem. Eng.*, 2022, **10**, 14240–14247.

26 A. Zubkiewicz, I. Irska, P. Miadlicki, K. Walkowiak, Z. Rozwadowski and S. Paszkiewicz, *J. Mater. Sci.*, 2021, **56**, 19296–19309.

27 C. H. R. M. Wilsens, Y. S. Deshmukh, B. A. J. Noordover and S. Rastogi, *Macromolecules*, 2014, **47**, 6196–6206.

28 Q. Zhang, M. Song, Y. Xu, W. Wang, Z. Wang and L. Zhang, *Prog. Polym. Sci.*, 2021, **120**, 101430.

29 Y. Jiang, D. Maniar, A. J. J. Woortman and K. Loos, *RSC Adv.*, 2016, **6**, 67941–67953.

30 J. Ma, X. Yu, J. Xu and Y. Pang, *Polymer*, 2012, **53**, 4145–4151.

31 C. Lavilla and S. Muñoz-Guerra, *Green Chem.*, 2013, **15**, 144–151.

32 S. Sun, Y. Xue, X. Xu, L. Ding, Z. Jiang, L. Meng, P. Song and Y. Bai, *Macromolecules*, 2021, **54**, 1254–1266.

33 D. L. Oatley-Radcliffe, M. Walters, T. J. Ainscough, P. M. Williams, A. W. Mohammad and N. Hilal, *J. Water Process. Eng.*, 2017, **19**, 164–171.

34 M. R. Esfahani, S. A. Aktij, Z. Dabaghian, M. D. Firouzjaei, A. Rahimpour, J. Eke, I. C. Escobar, M. Abolhassani, L. F. Greenlee, A. R. Esfahani, A. Sadmani and N. Koutahzadeh, *Sep. Purif. Technol.*, 2019, **213**, 465–499.

35 Y. Lv, Y. Du, Z. X. Chen, W. Z. Qiu and Z. K. Xu, *J. Mater. Sci.*, 2018, **545**, 99–106.

36 J. Alam, A. K. Shukla, M. A. Ansari, F. A. A. Ali and M. Alhoshan, *Membranes*, 2020, **11**(1), 25.

37 N. Haghighat, V. Vatanpour, M. Sheydaei and Z. Nikjavan, *Sep. Purif. Technol.*, 2020, **237**, 116374.

38 H. Barzegar, M. A. Zahed and V. Vatanpour, *J. Water Process. Eng.*, 2020, **38**, 101638.

39 J. H. Kim, C. Mun, J. Ma, S. G. Park, S. Lee and C. S. Kim, *Nanomaterials*, 2020, **10**(5), 949.